Sensors and Materials, Vol. 35, No. 8 (2023) 2807–2816
MYU Tokyo

S & M 3356

Use of Concave Sapphire Substrate to Synthesize ZnO Nanorod Arrays and Application of a Cu-decorated ZnO Nanorod Array Gas Sensor

Kai-Xu Han,[1,2] Jang-Cheng Jheng,[3] Wei Chien,[1,2]
Fang-Hsing Wang,[3*] and Cheng-Fu Yang[4,5**]

[1]Guangxi Key Laboratory of Ocean Engineering Equipment and Technology,
12 Binhai Avenue, Qinzhou 535011, China
[2]Key Laboratory of Beibu Gulf Offshore Engineering Equipment and Technology (Beibu Gulf University),
Education Department of Guangxi Zhuang Autonomous Region, 12 Binhai Avenue, Qinzhou 535011, China
[3]Graduate Institute of Optoelectronic Engineering, National Chung Hsing University,
145 Xingda Rd., South Dist., Taichung City 40227, Taiwan
[4]Department of Chemical and Materials Engineering, National University of Kaohsiung,
700, Kaohsiung University Rd., Nanzih District, Kaohsiung 811, Taiwan
[5]Department of Aeronautical Engineering, Chaoyang University of Technology,
168, Jifeng E. Rd., Wufeng District, Taichung 413310, Taiwan

(Received April 17, 2023; accepted July 27, 2023)

Keywords: Al-decorated ZnO, nanorod arrays, gas sensor, hydrothermal method

In this paper, a ZnO seed layer was deposited by spin coating on sapphire templates with patterned concave arrays used as substrates. Then, a hydrothermal method was used with a 0.03 M solution of $Zn(CH_3COO)_2{\cdot}2H_2O$, $CH_3OCH_2CH_2OH$, and C_2H_7NO to synthesize ZnO nanorod arrays on the surface of the ZnO seed layer at different synthesis times (30, 45, and 60 min). To evaluate the effect of Cu metal on enhancing the H_2 and CO gas sensing of the ZnO nanorods, the samples were divided into two groups: ZnO nanorod arrays without and with Cu decoration. We compared the photoluminescence properties of the arrays synthesized for the above durations, as well as those synthesized for 60 min both with and without Cu decoration. All ZnO nanorod arrays exhibited a distinct emission peak in the UV region at approximately 378 nm. However, the emission intensity of the ZnO nanorod arrays decorated with Cu was significantly higher than that of the undecorated nanorods. To fabricate a metal–semiconductor–metal gas sensor, we deposited 350-nm-thick interdigitated Cu electrodes on the ZnO nanorod arrays. The sensor was utilized to measure the concentrations of H_2 and CO across ranges of temperatures and concentrations (100 to 2000 ppm). We identified the optimal sensing parameters by comparing the results obtained from the ZnO nanorod arrays synthesized for 60 min with and without Cu decoration.

1. Introduction

In recent years, there has been a surge in research on zinc oxide (ZnO) and its derivatives owing to their widespread availability and nontoxic nature, as well as their ability to be grown at

*Corresponding author: e-mail: fansen@dragon.nchu.edu.tw
**Corresponding author: e-mail: cfyang@nuk.edu.tw
https://doi.org/10.18494/SAM4459

ISSN 0914-4935
https://myukk.org/

low temperatures and their greater stability than indium tin oxide (ITO) under H_2 plasma.[1] ZnO, especially in its 1D nanomaterial form as ZnO nanorods, has attracted significant interest owing to its advantageous optical, electrical, and mechanical properties and its cost-effectiveness in forming a 1D crystal structure. The development of selective growth technology is crucial for incorporating nanorods with different sizes and pitches into optoelectronic devices. However, as device sizes decrease and densities increase, the technology for selectively growing nanostructures must also advance. Moreover, the size requirements have progressed from micron and submicron to the nanoscale.

The surface area of ZnO nanomaterials primarily affects the adsorption criticality of reactive gases, as well as the conversion to high response amplitude and sensitivity. Controlled structures of the fabricated ZnO-based sensors facilitate oxygen adsorption and reactivity to change their electrical signals, thereby changing their sensing effects. Researchers have organized these fabrication processes and new types of architecture (1D, 2D, and 3D) into hierarchical structures,[2,3] despite their varied implementations.[4] Although the gas sensors fabricated using different structures have the same mechanism, which involves the interaction between O^- and O^{2-}, the primary interaction occurs between the reduced gas and the chemisorbed oxygen species.[5] The incorporation of noble metal catalyst nanoparticles into the metal–oxide–semiconductor structure of a sensor[6] further augments the chemical heterogeneity of the surface, thereby increasing the sensor's response. The addition of gold, silver, copper (Cu), aluminum, palladium, or platinum nanoparticles to ZnO nanorods elicits notable responses to specific gases such as hydrogen (H_2) and carbon monoxide (CO).

Liao *et al.* discovered that nanorods with smaller diameters exhibit a higher sensitivity owing to their larger surface area, which enhances the gas adsorption and reaction, resulting in an improved electrical response.[7] On this basis, they fabricated the ZnO nanostructure arrays on a protruding sapphire substrate. To improve the sensing capabilities of ZnO nanostructures, various copper-based nanoparticles have been used to decorate their surfaces. Tohidi *et al.* decorated ZnO nanorods with CuO and demonstrated the significant impact of this decoration on the performance of CO gas sensing.[8] Mollaha and Tohidi used Cu_2O to decorate ZnO nanotubes and found that the decorated ZnO nanotubes had improved sensitivity and feasibility for detecting CO gas compared with undecorated ZnO nanotubes.[9,10]

ZnO-based materials are suitable for the production of H_2 sensors. Al-Hardan *et al.* utilized a Zn film and controlled the oxidation time to modify the electronic surface states, resulting in a variation in electron concentration. They employed this approach to evaluate the impact of the duration of oxidation of the ZnO film on the detection of H_2 gas.[11] To further enhance the sensing capabilities of ZnO nanorods, we investigated an innovative method of synthesizing ZnO nanorods into ZnO nanorod arrays. The second novelty is that we decorated their surfaces with Cu nanoparticles and compared the efficiencies of Cu-decorated and undecorated ZnO nanostructures for detecting CO and H_2. The results indicated that ZnO nanorod arrays decorated with Cu exhibited a higher sensitivity to these gases than the undecorated arrays. In this study, we conducted measurements at different temperatures ranging from 50 to 300 °C and gas concentrations ranging from 100 to 2000 ppm to determine the optimal operating conditions for gas detection.

2. Experimental Procedure

In this study, a sapphire template with a patterned concave structure, as shown in Fig. 1, was used as the substrate. After the substrate was cleaned, a ZnO seed layer was coated on it by spin coating. Figures 1(a) and 1(b) depict the top-view and cross-sectional morphologies of the 2-inch sapphire substrate, respectively. The sapphire substrate contained concave nanostructures with an average bottom width of 0.3 μm and an average height of 0.5 μm. Additionally, a side view of the substrate is schematically illustrated in Fig. 2(a). To deposit the ZnO seed layer on the substrate, spin coating was employed six times, as shown in Fig. 2(b). Then, upon the completion of the ZnO film coating, the substrate underwent annealing at 500 °C for 1 h to improve the crystallinity of the ZnO seed layer. ZnO nanorod arrays were then synthesized for 30, 45, or 60 min via the hydrothermal method with a 0.03 M solution of zinc acetate ($Zn(CH_3COO)_2{\cdot}2H_2O$), $CH_3OCH_2CH_2OH$, and the conditioning agent $C_6H_{12}N_4$, as illustrated in Fig. 2(c). To fabricate a Cu-decorated ZnO nanorod array gas sensor, a 5-nm-thick layer of Cu metal was plated on the ZnO nanorod arrays by evaporation, as illustrated in Fig. 2(d). To convert the deposited Cu film

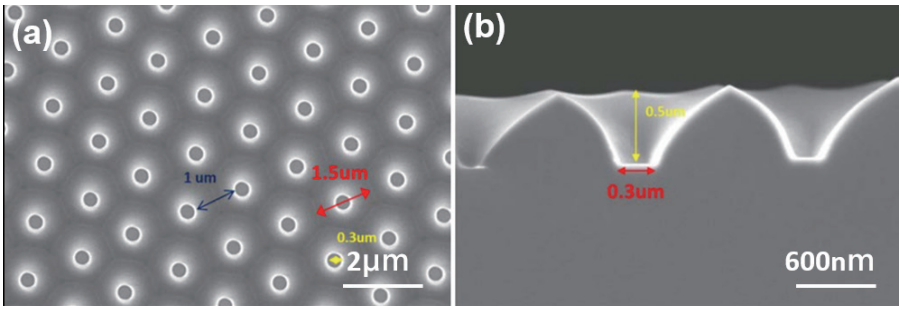

Fig. 1. (Color online) (a) Top and (b) side views of sapphire substrate with patterned concave structure.

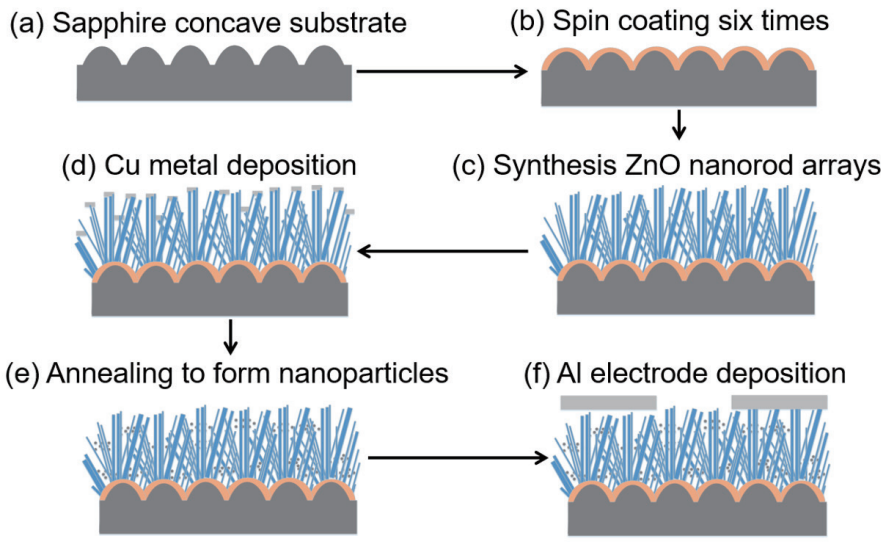

Fig. 2. (Color online) Schematic for fabrication of a Cu-decorated ZnO nanorod array gas sensor.

into Cu nanoparticles, the Cu-deposited ZnO nanorod arrays were annealed at 900 °C for 10 min while Ar was introduced to prevent oxidation, as shown in Fig. 2(e). The sensor's upper electrode was then plated with Al and primarily consisted of an interdigitated structure, as depicted in Fig. 2(f).

After synthesizing ZnO nanorod arrays on ZnO seed layers, we measured their X-ray diffraction spectra to analyze their crystalline phases. Additionally, we used field-emission scanning electron microscopy to observe the surface morphologies of the synthesized ZnO nanorod arrays. The photoluminescence (PL) properties of the ZnO nanorod arrays were measured at room temperature using a Hitachi F-4500 fluorescence spectrophotometer, with measurements taken in the range of 350–650 nm. After depositing Al electrodes on the ZnO nanorod arrays, the devices underwent pretreatment at 350 °C for 1 h while air was passed through the measurement chamber. A Keithley 2400 source meter was used to supply voltage and record measured data via a computer connection. The chamber was evacuated to 10^{-2} Torr, and the cavity was heated directly to 300 °C. Table 1 shows the parameters of the gas used for measurement. The desired measurement gas concentrations were controlled by adjusting the inlet gas flow. The gas concentration measurement was affected by factors such as the ventilation time, the flow rate of the mass flow control (*MFC*), the concentration of the gas cylinder, and the internal volume of the chamber. The formula for calculating the gas concentration is

$$Gc\ (\text{ppm}) = \frac{MFC \times L \times 60}{S \times C(\%) \times 1000}, \tag{1}$$

where *Gc*, *S*, *C*, *L*, and *MFC* respectively represent the required gas concentration, ventilation time, gas cylinder concentration (fixed value), cavity volume, and flow rate of the *MFC* (measured in sccm). By adjusting the flow rate of the *MFC* and the feeding time, the concentration of the gas to be measured could be set accordingly, as shown in Table 1.

3. Results and Discussion

A seed layer of ZnO was formed on the sapphire substrate concaves through six rounds of spin coating. Upon annealing at 300 °C, the spin-coated ZnO gel was transformed into nanoscale crystalline particles, as indicated in Fig. 3. The average thickness of the resulting film was approximately between 160 and 238 nm, with a deposition rate of around 26.7 to 40 nm per coating. The XRD pattern of the 45-min-synthesized ZnO nanorod arrays is depicted in Fig.

Table 1
Concentration and other parameters of the measured gas.

Preset concentration (ppm)	Inlet gas flow (sccm)	Inlet gas time (s)
100	50	5
500	200	6.25
1000	200	12.5
1500	200	18.75
2000	200	25

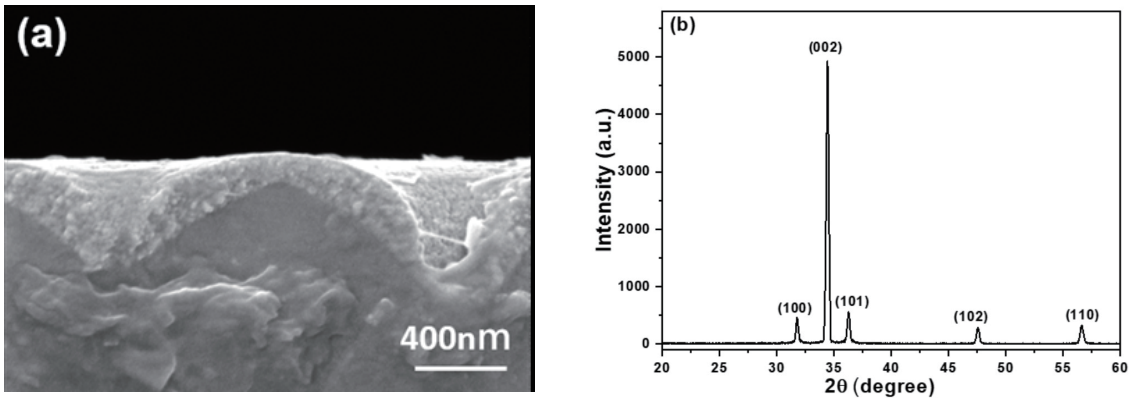

Fig. 3. (Color online) (a) SEM image of prepared ZnO seed layer. (b) XRD pattern of 45-min-synthesized ZnO nanorod arrays.

3(b), revealing a dominant diffraction peak on the (002) plane with additional diffraction peaks on the (100), (101), (102), and (110) planes. This result suggests that the crystallization of ZnO nanorod arrays has a preferential orientation along the *c*-axis. The Debye–Scherrer equation, $D = (k\lambda/\beta \cos \theta)$, is used to determine the size of nanoscale crystalline particles.[12] By substituting the θ and full width at half maximum (FWHM) values of the (002) diffraction peak shown in Fig. 3(b) into the Debye–Scherrer equation, the grain size of the 45-min-synthesized ZnO nanorod arrays was directly calculated to be approximately 28.9 nm. The XRD patterns and grain sizes of the 30- and 60-min-synthesized ZnO nanorod arrays were similar to those of the 45-min-synthesized ZnO nanorod arrays, an explanation for which will be provided later.

Figure 4 shows the surface morphologies of ZnO nanorod arrays grown on sapphire substrates featuring a concave surface. The arrays were synthesized using a ZnO seed layer at various synthesis times. From this figure, the measured average diameters were 52 nm (ranging from 48 to 57 nm), 74 nm (71 to 78 nm), and 89 nm (86 and 93 nm). Figure 5 shows the cross-sectional morphologies of ZnO nanorods synthesized for different lengths of time. The SEM images in Fig. 5 show that the synthesized ZnO nanorods form at the structure of ZnO nanorod arrays. From this figure, the measured average lengths of the ZnO nanorod arrays synthesized for 30, 45, and 60 min were 407 nm (lengths ranging from 390 to 431 nm), 511 nm (489 to 536 nm), and 551 nm (529 to 573 nm), respectively. Both the average length and diameter of the ZnO nanorod arrays increased with the synthesis time. In addition, the careful control of parameters such as the growth time and solution concentration in the hydrothermal method is necessary to prevent the fusion of nanorods. In the early stages of growth, the lower portions of the fine ZnO nanorods came in contact with each other, leading to the fusion of the entire bundle into a larger hexagonal ZnO nanorod. This was attributed to the reduction in surface energy during the synthesis of the ZnO nanorod arrays. Interestingly, the average lengths of the ZnO nanorod arrays synthesized for 45 and 60 min were similar.

The results in Fig. 5 show that increasing the synthesis time does not result in an apparent increase in the length of the ZnO nanorods. However, during the synthesis, adjacent nanorods combine to form larger nanorods, leading to an increase in nanorod diameter and a decrease in

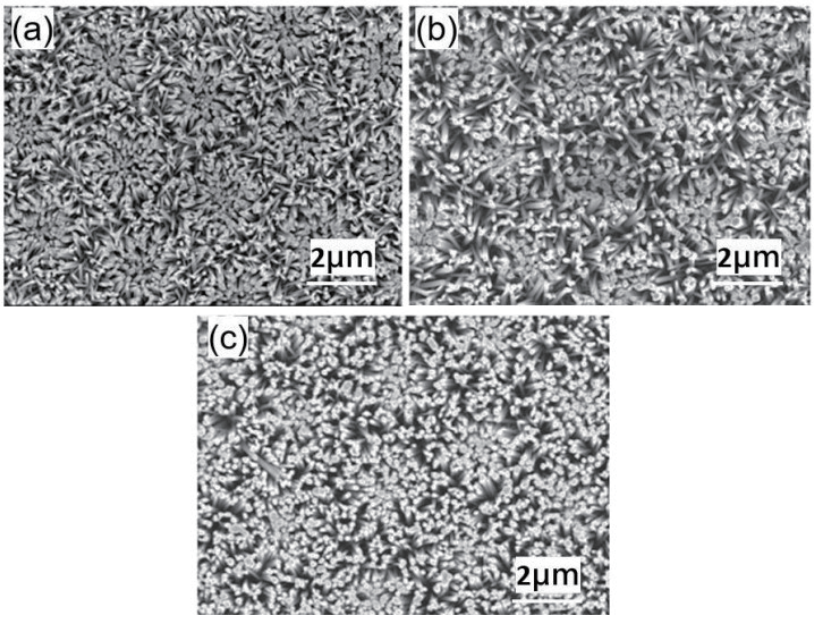

Fig. 4. (Color online) Surface morphologies of ZnO nanorod arrays with synthesis times of (a) 30, (b) 45, and (c) 60 min.

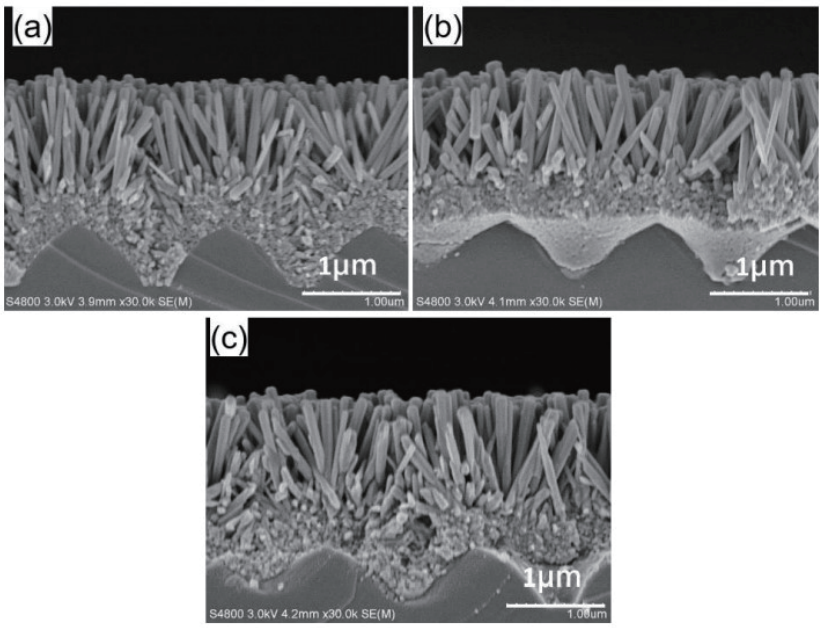

Fig. 5. (Color online) Cross-sectional morphologies of the ZnO nanorod arrays with synthesis times of (a) 30, (b) 45, and (c) 60 min.

nanorod density. We determined the density of ZnO nanorods by selecting five points from the middle, right, left, top, and bottom of SEM images. A square with an area of 1 μm^2 was then drawn around each of the five points, and the number of ZnO nanorods in each square was counted.[13,14] For synthesis times of 30, 45, and 60 min, the average numbers of ZnO nanorods in 1 μm^2 were 125, 116, and 48, respectively. As the growth time increased, the density of ZnO

nanorods decreased and the diameter increased. The total surface area and the surface area of the tops of the ZnO nanorods in each square were also calculated to be on average 7.2, 14.2, and 20.6 μm^2 and 0.18, 0.36, and 0.51 μm^2 for synthesis times of 30, 45, and 60 min, respectively. Consequently, the average volumes of ZnO nanorods in each square were 0.37, 1.05, and 1.83 μm^3, respectively. Table 2 presents a summary of the results for the synthesized ZnO nanorod arrays for the three synthesis times. Because the ZnO nanorods synthesized for 60 min had the largest surface area per unit area, they were subsequently used as the sensing material for the gas sensor in this study.

In wavelength bands other than UV, luminescence is caused by defects in the crystal lattice of zinc and oxygen. In 1996, Vanheusden *et al.* proposed a mechanism for green light emission in ZnO that involves the recombination of oxygen vacancies and holes generated by photoexcitation.[2] Govender *et al.* have shown that the concentration of oxygen vacancies in ZnO affects the intensity of green light emission.[16] The results of these previous studies also confirm that oxygen vacancies in ZnO are responsible for green light emission. Synthesized ZnO nanorods typically exhibit various types of defect, with the PL spectrum being a crucial tool for comparing and characterizing them. Figure 6(a) depicts the PL spectra of the ZnO nanorod arrays synthesized for different durations and excited using UV with a 325 nm wavelength. These ZnO arrays displayed a clear emission peak in the UV region at around 378

Table 2
Summary of dimensions of ZnO nanorods grown on sapphire substrates with concaves for different synthesis times.

Synthesis time (min)	30	45	60
Length (*L*, nm)	407	511	551
Diameter (*D*, nm)	52	74	89
Aspect ratio, *L*/*D*	7.8	6.9	6.2
Total top surface area (μm^2)	0.18	0.36	0.51
Total surface area (μm^2)	7.2	14.2	20.6
Density (μm^{-2})	125	116	48

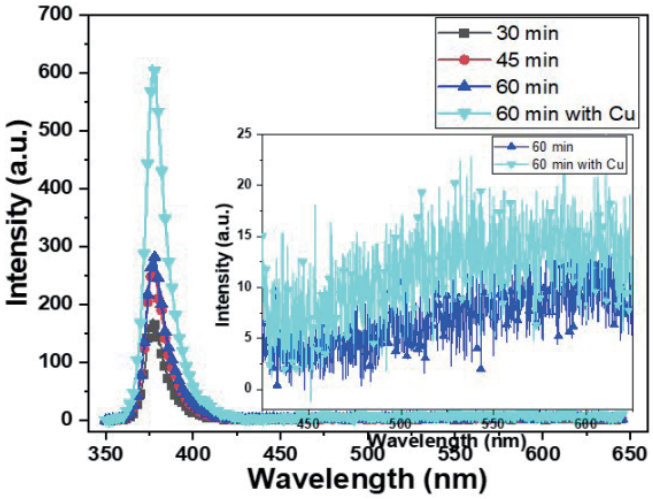

Fig. 6. (Color online) PL spectra of ZnO nanorod arrays fabricated with different synthesis times and 60-min-synthesized ZnO nanorods with Cu decoration.

nm, which resulted from the recombination of free excitons within the ZnO crystal lattice, also known as near-band edge emission. Additionally, there was an indistinct emission peak in the visible green region that arose from defects formed during the synthesis of the arrays, which may have resulted from lattice strain, impurities, or oxygen vacancies. Figure 6 reveals that the intensity of the UV peak increased with the synthesis time, whereas that of the visible green emission remained relatively constant. This indicates that the volume of defects in the ZnO nanorod arrays did not significantly increase with the synthesis time. The increase in UV emission intensity can be primarily attributed to the increased diameter and length of the ZnO nanorods over time, leading to increases in top surface area and total volume and, consequently, an increase in UV peak intensity. Figure 6 also includes the PL spectrum of the ZnO nanorod arrays synthesized for 60 min with Cu decoration, and Table 3 provides a comparison of the emission intensities of the peak at around 378 nm and the peak in the visible green region for 60-min-synthesized ZnO nanorod arrays without and with Cu decoration. The UV emission intensity of the Cu-decorated ZnO nanorod arrays was higher than that of the undecorated ones. These findings suggest that Cu decoration alters the PL characteristics of ZnO nanorod arrays, which can impact their sensing abilities towards gases such as H_2 and CO.

By varying the measurement time, we observed changes in the resistance and resistance response of the nanorod arrays when introducing H_2 and CO gases at a concentration of 2000 ppm, as well as air. The results are presented in Fig. 7(a). The times required for the resistance to drop or rise by 90% of the difference between the initial and lowest or highest resistance values after gas or air introduction are defined as the reaction and recovery times. The resistances of the ZnO nanorod arrays with and without Cu decoration were measured in air at 50 °C (300 °C)

Table 3
Comparison of the emission intensities of the peak at around 378 nm and the peak in the visible green region for 60-min-synthesized ZnO nanorod arrays without and with Cu decoration. I_{UV}: emission intensity of the peak at around 378 nm, I_G: emission intensity of the peak in the visible green region.

Time (min)	I_{UV}	average I_G	I_G/I_{UV}
Undecorated	281.5	8.24	0.0293
Cu-decorated	604.4	14.2	0.0235

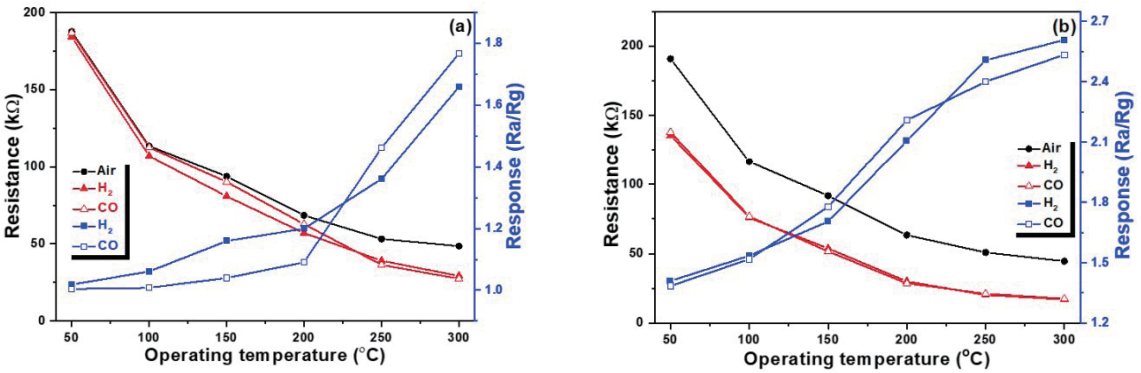

(a) (b)

Fig. 7. (Color online) Temperature-dependent resistance and resistance response of gas sensor at the gas concentration of 2000 ppm. (a) ZnO nanorod arrays and (b) Cu-decorated ZnO nanorod arrays.

to be 187.6 and 190.8 kΩ (48.6 and 44.6 kΩ), respectively. These results suggest that the Cu decoration does not significantly affect the resistance of the ZnO nanorod arrays in air. However, upon introducing H_2 and CO gases, there was no significant change in the resistance of the ZnO nanorod arrays without Cu decoration at 50 °C, whereas the resistance of the ZnO nanorod arrays with Cu decoration decreased to approximately 135 kΩ. This indicates that Cu metal can act as a catalyst, enhancing the responses to H_2 and CO gases.

Figure 7(b) shows that the differences in resistance between the Cu-decorated ZnO nanorod arrays at 50 and 300 °C are similar when H_2 and CO gases are introduced. This finding confirms that Cu-decorated ZnO nanorod arrays exhibit stable catalytic properties, even at high temperatures. Additionally, Fig. 7(b) reveals that the response ratio of the ZnO nanorod arrays without Cu decoration increases slightly with temperature below 200 °C but increases rapidly above 200 °C. Conversely, the response ratio of the Cu-decorated ZnO nanorod arrays increases linearly as the temperature increases from 50 to 300 °C. These results demonstrate that Cu-decorated ZnO nanorod arrays exhibit superior sensing properties to undecorated ZnO nanorod arrays for H_2 and CO gases.

At 300 °C, controlling the H_2 and CO concentrations between 100 and 2000 ppm results in changes in resistance and resistance response. When introduced to argon, the resistance decreases from the initial measured value of 44.6 kΩ in air. This is mainly due to an increase in the number of gas molecules that react with oxygen, releasing electrons and increasing the resistance response proportionally to the gas concentration. Figures 8(a) and 8(b) demonstrate the relationship between the CO and H_2 concentrations and the measured resistance and resistance response. At H_2 concentrations of 100, 500, 1000, 1500, and 2000 ppm, the measured resistances were 31.6, 28.2, 25.1, 22.5, and 17.1 kΩ, with resistance responses of 1.41, 1.58, 1.77, 1.98, and 2.60, respectively. At CO concentrations of 100, 500, 1000, 1500, and 2000 ppm, the measured resistances were 32.9, 28.5, 25.3, 22.0, and 17.6 kΩ with corresponding resistance responses of 1.35, 1.56, 1.76, 2.02, and 2.53, respectively. The results indicate that the detection performance of a ZnO nanorod array gas sensor is dependent on the concentration of the target gas. Specifically, a higher gas concentration leads to a greater resistance response.

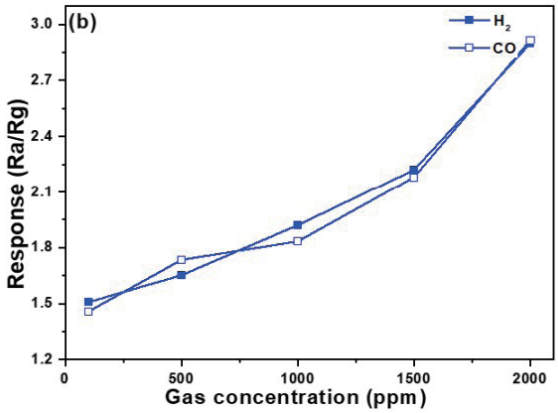

Fig. 8. (Color online) (a) Resistance and (b) resistance response of a ZnO nanorod array gas sensor decorated with Cu and grown for 60 min for CO and H2 concentrations from 100 to 2000 ppm at 300 °C.

4. Conclusions

In this study, a sapphire template with an array of concaves was used as a substrate, on which a ZnO seed layer was deposited and ZnO nanorod arrays were synthesized. We investigated the effectiveness of the nanorod arrays as sensors of CO and H_2 gases for both undecorated arrays and arrays decorated with Cu. The resistances of ZnO nanorod arrays with and without Cu decoration were measured in air and at 50 °C (or 300 °C), resulting in values of 187.6 and 190.8 kΩ (or 48.6 and 44.6 kΩ), respectively. When H_2 (CO) concentrations were 100, 500, 1000, 1500, and 2000 ppm, the measured resistances were 31.6 (32.9), 28.2 (28.5), 25.1 (25.3), 22.5 (22.0), and 17.1 (17.6) kΩ, with corresponding resistance response values of 1.41 (1.35), 1.58 (1.56), 1.77 (1.76), 1.98 (2.02), and 2.60 (2.53), respectively. The results demonstrate that the detection performance of a ZnO nanorod array gas sensor relies on several factors, including the concentration of the target gas, the testing temperature, and the presence of Cu decoration. The increased gas concentration and higher testing temperatures result in a more pronounced resistance response. Notably, the implementation of Cu decoration on the surfaces of ZnO nanorod arrays significantly enhances the resistance response of the gas sensor.

Acknowledgments

This work was supported by projects under Nos. MOST 110-2622-E-390-002, MOST 110-2221-E-390-020, and MOST 111-2221-E-390-018.

References

1 C. C. Tsai and S. P. Huang: Inter. Con. Safety & Security Management and Engineering Technology (ICSSMET2010) **2** (2010).
2 K. Vanheusden, W. L. Warren, C. H. Seager, D. R. Tallant, and J. A. Voigt: J. Appl. Phys. **79** (1996) 7983.
3 F. Li, Z. Li, and F. J. Jin: Mater. Lett. **61** (2007) 1876.
4 B. Lin, Z. Fu, Y. Jia, and G. Liao: J. Electrochem. Soc. **148** (2001) 110.
5 M. S. Arnold, P. Avouris, and Z. W. Pan: J. Phys. Chem. B **107** (2003) 659.
6 Y. C. Wang: Electro. Chem. Solid-State Lett. **5** (2002) C53.
7 L. Liao, H. B. Lu, J. C. Lin, and C. Lin: J. Phys. Chem. C **111** (2006) 1900.
8 S. Tohidi, T. Tohidi, and P. H. Mohammadabad: J. Mole. Model. **27** (2021) 279.
9 M. Mollaha and T. Tohidi: J. Electron. Mater. **51** (2022) 7143.
10 O. Alev, N. Sarıca, O. Ozdemir, L. C. Arslan, S. Buyukkose, and Z. Z. Ozturk: J. Alloys Compd. **826** (2020) 154177.
11 N. Al-Hardan, M. J. Abdullah, and A. Abdul Aziz: Appl. Surf. Sci. **255** (2009) 7794.
12 C. C. Chen, F. H. Wang, S. C. Chang, and C. F. Yang: Materials **11** (2018) 1501.
13 C. F Yang, C. S. Wang, F. H. Wang, H. W. Liu, and J. Micova: Appl. Funct. Mater. **2** (2022) 44.
14 C. Y. Lee, C. S. Wang, F. H. Wang, H. W. Liu, and C. F. Yang: ACS Omega **7** (2022) 17384.
15 R. A. Laudise and A. A. Ballman: J. Phys. Chem. **64** (1960) 688.
16 K. Govender, D. S. Boyle, P. B. Kenway, and P. O'Brien: J. Mater Chem. **14** (2004) 2575.